American Mineralogist, Volume 59, pages 1069–1082, 1974

The High Temperature Crystal Chemistry of Clinohypersthene[1]

JOSEPH R. SMYTH

Lunar Science Institute[2], 3303 Nasa Road 1, Houston, Texas 77058

Abstract

Single crystal X-ray intensity data have been obtained from a crystal of clinohypersthene, $Mg_{0.31}Fe_{0.67}Ca_{0.015}SiO_3$ at 20°, 200°, 400°, 600°, 700°, 760° and 825°C. Refinements of the crystal structure using three dimensional data and anisotropic thermal models have been made at each temperature. Clinohypersthene undergoes a first-order transition from space group $P2_1/c$ to $C2/c$ at 725° ± 10°C. Cell dimensions indicate a discontinuous change in the length of the axis of greatest thermal expansion at the transition. The $h + k$ odd diffractions remain sharp and observable up to the temperature of transition and exhibit a discontinuous drop to zero intensity at the transition. The high clinopyroxene refinements appear to represent a real structure rather than an average of the two primitive silicate chain configurations. There are slight tendencies for clinohypersthene to exhibit more ordering of Mg and Fe on $M1$ and $M2$ and for Fe–Mg exchange to begin at higher temperatures and to have a slightly higher ΔG of exchange than does orthopyroxene.

Introduction

In the pyroxene quadrilateral, the low-Ca clinopyroxene structure (space group $P2_1/c$) occurs with compositions ranging from pure enstatite ($MgSiO_3$) to about $En_{12}Fs_{88}$ and may contain up to 15 mole percent wollastonite ($CaSiO_3$). The structure has been shown to be distinctly different from the high-Ca clinopyroxenes, augite, diopside, and hedenbergite (space group $C2/c$, Morimoto, 1956; Morimoto, Appleman, and Evans, 1960). In the $P2_1/c$ structure, the $M2$[3] site is 6-coordinated, while in the $C2/c$ high Ca structure it is 8-coordinated, so that the $P2_1/c$ structure more closely resembles orthopyroxene in the first coordination of cations and density of symmetry elements, than it does the high Ca clinopyroxenes. The $P2_1/c$ structure has been shown to undergo a reversible, non-quenchable, displacive transition to space group $C2/c$ in the temperature range from 700° to 1050°C, depending upon composition. This transition was predicted by Morimoto and Tokonami (1969) and Smith (1969), and verified experimentally by high temperature single crystal X-ray studies by Smyth (1969) and Prewitt, Papike, and Ross (1970). The structure of the high temperature form has been determined by Smyth and Burnham (1972) for the composition $En_{31}Fs_{67}Wo_{1.5}$, and by Brown *et al* (1972a) for the composition $En_{65}Fs_{30}Wo_5$. The coordination of $M2$ within this structure differs distinctly both from that of the low temperature form and from the augite structure. The general nature of the high temperature structure is now well understood. However, the nature of the transition is not well understood and there remain some unanswered questions of petrologic significance.

Perhaps the most significant question about this $P2_1/c$ to $C2/c$ transition is its order. A first-order transition might give rise to a two-phase field of finite width in temperature-composition space which could result in rocks containing two low-Ca clinopyroxenes of different compositions. From structure determinations, it is known that the coordination of $M2$ to bridging oxygens changes, but it is not known whether this transition is first order, as is the clino-to-proto transition (Smyth, 1974), or of higher order as the $P\bar{1}$ to $I\bar{1}$ transition in anorthite (Foit and Peacor, 1973). This question can best be answered by a close monitoring of the $h + k$ odd intensities as the crystal undergoes the transition. Related to the order of the transition is the question of whether the high temperature structure represents a real configuration or merely a disordered average of the

[1] The Lunar Science Institute Contribution No. 180.

[2] The Lunar Science Institute is operated by the Universities Space Research Association under Contract No. NSR 09-051-001 with the National Aeronautics and Space Administration.

[3] Nomenclature of Burnham *et al* (1967) used throughout.

two chains of the primitive structure similar to $I\bar{1}$ anorthite reported by Foit and Peacor (1973). This would be best answered by full anisotropic refinement of the high temperature form .

For many natural pigeonites, particularly Ca-rich pigeonites of volcanic origin, the $h + k$ odd diffractions are diffuse relative to the $h + k$ even. Selective diffuseness of subsymmetry diffractions has generally been attributed to the small size of domains over which the short-range order of the low-symmetry cell is maintained. If the domain size is a function only of the amount of time allowed for nucleation and growth of domains in the solid state, the diffuseness may be a useful indicator of cooling rates (Brown, Papike, and Prewitt, 1972b). However, the very low Ca sample which Smyth and Burnham (1972) quenched to 20°C from 900°C in a few seconds showed no diffuseness of the $h + k$ odd diffractions. It may be that the domain size in the natural volcanic specimens is controlled by very fine scale Ca-rich lamellae rather than by cooling rate, thus making the diffuseness of the $h + k$ odd diffractions more a function of Ca-content than of cooling rate. Precise measurement of the shapes of the diffraction maxima after crossing the $C2/c$ to $P2_1/c$ transition at various cooling rates should clarify the effects of cooling rate on the selective diffuseness of the $h + k$ odd diffractions. Brown *et al* (1972a) and Prewitt, Brown, and Papike (1971) report a hysteresis effect of the P to C transition temperature and a gradual decrease in the temperature of the transition after prolonged heating, but Smyth and Burnham (1972) report no hysteresis in the P to C inversion in their low Ca clinopyroxene. Further detailed study may help to explain this phenomenon.

The orthopyroxene structure has been studied in detail at a series of temperatures (Smyth, 1973, at $En_{31}Fs_{67}Wo_{1.5}$ and Sueno, Cameron, and Prewitt, 1973, at Fs_{100}). A similarly detailed study of a low Ca clinopyroxene for comparison should reveal much about the relative stabilities of these two closely related structures as well as about Fe–Mg ordering on the $M1$ and $M2$ sites in the high temperature clinopyroxenes.

TABLE 1. Details of Intensity Measurements and Structure Refinements

TEMPERATURE (°C) ± 10°C)	20	200	400	600	700	760	825
Crystal #	1	2	2	3	3	3	3
Preheat time (hrs.)		12	12	24	24	12	12
Radiation	Mo	Mo	Mo	Mo	Mo	Mo	Mo
Filter	Nb	Nb	Nb	*	*	*	*
Monochromator	*	*	*	Gr**	Gr	Gr	Gr
KV/MA	36/16	36/16	36/16	40/16	40/16	40/16	40/16
2θ scan speed (°/min.)	1.0	2.0	2.0	2.0	2.0	2.0	2.0
Maximum 2θ (°)	90	50	50	50	50	60	60
Number of Measurements	1555	872	884	784	785	665	669
Number observed (>3σ)	1481	590	602	254	248	200	240
Final Weighted R	.037	.050	.052	.034	.044	.036	.035

* None used.
** Graphite curved crystal, 2θ = 11.8°.

Experimental

A clinopyroxene formed by inversion from natural orthopyroxene was used for this study in order to permit direct comparison between orthopyroxene and clinopyroxene structures at temperature, and also to be free of the effects of large amounts of Ca (*i.e.*, augite exsolution). The clinopyroxene crystals were prepared by heating a natural metamorphic orthopyroxene at 990°C for three days in an evacuated silica-glass capsule. The clinopyroxene thus formed was found to be identical in composition to the original orthopyroxene by microprobe analyses (cations per six oxygens): Si, 1.997; Ti, 0.002; Al, 0.005; Mg, 0.636; Fe, 1.327; and Ca, 0.032. This material is that used for the determination of the high and low clinohypersthene structures (Smyth and Burnham, 1972), and for the high temperature structure of orthopyroxene (Smyth, 1973).

A crystal of this clinohypersthene was mounted in an evacuated silica-glass capillary and oriented on a Picker FACS-1 automated X-ray diffractometer. The crystal was heated to 200° ± 10°C using a heating stage similar to that described by Smyth (1972), and allowed to equilibrate for 12 hours before intensity measurement began. All symmetry-independent intensities of 2θ less than 50° were measured, then the crystal temperature was increased to 400°C. After re-equilibrating for 12 hours, the same set of intensities was re-measured. Because of a faulty seal in the capillary, the first crystal began to oxidize when heated to 600°C; therefore a second crystal was mounted and heated to 600°C for 24 hours, and an equivalent set of intensities was measured. This crystal was then used for data collections at 700°, 760°, and 825°C in a similar manner, except that the intensities with indices $h + k$ odd were not systematically measured at 760° and 825°C as they were found to be extinct. Details of intensity measurements at each temperature are presented in Table 1. After the data collection at 825°C, the crystal was cooled to 20°C and showed no signs of

TABLE 2. Unit Cell Parameters at Various Temperatures

	TEMPERATURE (°C ± 10°C)										
	20	200	400	500	600	700	720	730	740	760	825
a (Å)	9.691(3)*	9.709(2)	9.720(5)	9.734(5)	9.762(4)	9.794(4)	9.807(3)	9.826(9)	9.839(9)	9.851(4)	9.870(5)
b (Å)	8.993(3)	9.008(3)	9.027(6)	9.034(6)	9.046(5)	9.057(4)	9.056(3)	9.048(10)	9.046(11)	9.045(5)	9.054(5)
c (Å)	5.231(2)	5.234(1)	5.248(3)	5.257(3)	5.268(2)	5.279(3)	5.286(2)	5.314(6)	5.311(7)	5.326(3)	5.328(3)
β (°)	108.61(2)	108.80(1)	108.88(2)	108.98(3)	109.16(3)	109.35(3)	109.47(2)	109.73(6)	109.83(7)	110.05(3)	110.15(3)
Vol.(Å^3)	432.0(2)	433.4(1)	435.7(2)	437.1(3)	439.5(3)	441.8(3)	442.6(2)	444.7(6)	444.7(6)	445.8(3)	447.1(3)

* Parenthesized figures represent the estimated standard deviation (esd) in terms of the least units for the value to their immediate left, thus 9.691(3) indicates an esd of 0.003. This notation for esd is used consistently throughout this work.

oxidation. A final set of data ($2\theta < 50°$) was collected at 20°C for comparison.

Cell dimensions of the crystal were determined by careful manual centering of ten strong diffractions and subsequent least-squares refinement of the cell parameters from these data at the following temperatures: 20°, 200°, 400°, 500°, 600°, 700°, 720°, 730°, 740°, 760°, and 825°C (Table 2). The shapes and intensities of the eight strongest diffractions with $h + k$ odd and four representative diffractions with $h + k$ even were measured at each of the above temperatures. The intensities of the peaks in each group were averaged and are plotted as a function of temperature in Figure 1. The shapes of a typical peak of each type at several different temperatures are plotted in Figure 2.

As shown in Figure 1, the intensities of the $h + k$ odd diffractions went abruptly to zero at 725° ± 10°C and no intensity from any of these diffractions was observed at 730° ± 10°C and above. Figure 2 shows that the peaks remained sharp right up to the transition. The diffraction phenomena near the transition temperature were reexamined after data col-

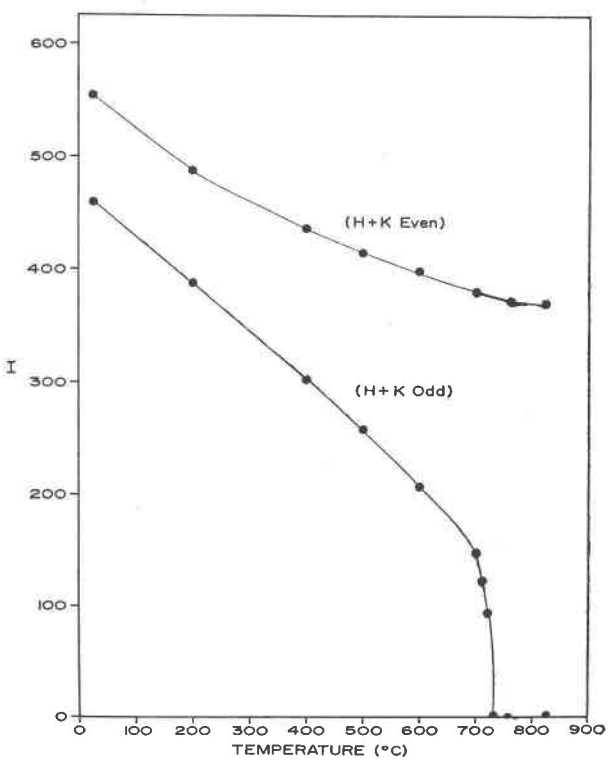

FIG. 1. Plot of the mean of representative $h + k$ odd and even diffractions as a function of temperature. The $h + k$ even diffraction monitored are *062*, *404*, *28$\bar{3}$*, and *66$\bar{2}$*. The $h + k$ odd diffractions are *102*, *304*, *23$\bar{1}$*, *05$\bar{2}$*, *70$\bar{2}$*, *23$\bar{3}$*, *23$\bar{5}$*, *30$\bar{4}$*, and *70$\bar{4}$*.

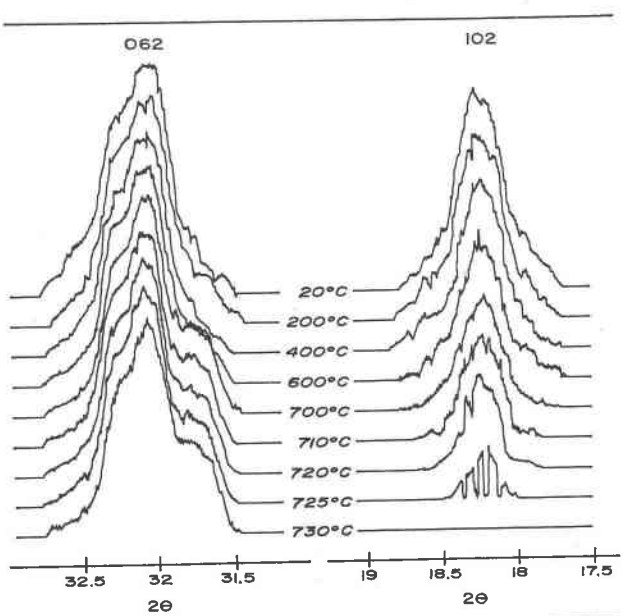

FIG. 2. Nested 2θ scans of representative $h + k$ odd and even intensities at several temperatures. There is no apparent difference in the sharpness of the two peaks. The *102* peak at 725°C is broken indicating that the crystal crossed the transition $P2_1/c$ to $C2/c$ several times during the 2θ scan. Similar behavior was observed in other $h + k$ odd diffractions at 725°C.

lection at 825°C was terminated. No change in the inversion temperature (725° ± 10°C) was observed after the crystal had been held above the transition for approximately 72 hours. The transition temperature was crossed at different cooling rates: first by a rapid quench to 20°C from 825°C in less than one second, and second at a cooling rate of approximately one degree per minute. At no time was any diffuseness observed of the $h + k$ odd relative to the $h + k$ even diffractions.

Structure Refinements

All sets of integrated intensities were corrected for Lorentz and polarization effects. Each intensity measurement was also corrected for absorption differences using numerical integration techniques (Burnham, 1966). Based on a linear absorption coefficient of 54.7 cm^{-1}, the transmission factors varied from 0.33 to 0.47 for the first crystal and 0.26 to 0.38 for the second. All refinements of the structure models were done with a slightly modified version of the full-matrix least-square refinement program RFINE (Finger, 1969). All observations were weighted according to $w = 1/\sigma_F^2$ where σ_F is the standard deviation of the intensity measurement based on counting statistics as described by Burnham *et al* (1971). All observations below the minimum observable level (3σ) were rejected from the normal equations matrix during refinement of the model. Atomic scattering factors used are those for fully ionized cations and O^{-1} given by Cromer and Mann (1968) as derived from Hartree-Fock wave functions neglecting relativistic effects. In addition, both real and imaginary anomalous dispersion terms (*International Tables for X-ray Crystallography*, Vol. 3, p. 215) were included in the final cycles of refinement at each temperature. Throughout all refinements, the chemistry was constrained to the totals given in the chemical analyses. All Ca was fixed in *M*2, and Mg and Fe were allowed to partition between *M*1 and *M*2.

The initial structure model used for refinement of the low clinohypersthene, $P2_1/c$, structures at 200°, 400°, 600°, and 700°C was that given by Smyth and Burnham (1972). Four cycles of refinement, using isotropic thermal parameters, were performed for each temperature successively, using the results of the next lower temperature as a starting model. After four additional cycles of least squares refinement with anisotropic thermal parameters at each temperature, each structure had reached convergence. A similar procedure was followed for the high temperature, $C2/c$ structures at 760° and 825° using the high clinohypersthene structure determined by Smyth and Burnham (1972) at 950°C. Four cycles of refinement of the structure at 20°C after heating were performed using isotropic thermal parameters and the room temperature structure as an initial model. The structure was found to be identical to the initial model within the limits of error.

Final weighted R factors for each refinement are presented in Table 1. Final fractional atomic coordinates, equivalent isotropic temperature factors, and Fe, Mg, and Ca occupancies of *M*1 and *M*2 for refinements at each temperature are presented in Table 3.

Discussion

The Order of the Transition

The change in cell parameters with temperature (Table 2) indicates that the transition occurs at a discrete temperature. Cell volumes are plotted as a function of temperature in Figure 3. Plotting of the cell edges versus temperature is an inadequate means of describing the thermal expansion of a monoclinic crystal (Ohashi and Burnham, 1973). Using the method described by Ohashi (1973), the axial lengths and orientations of the thermal expansion ellipsoids were calculated between 20°C and the various temperatures at which cell edges were measured. Axis lengths versus temperature are plotted in Figure 4. In a monoclinic crystal (second setting), one of the axes of the thermal expansion ellipsoid is constrained by symmetry to be colinear with the b crystallographic axis, but the other two axes are free to lie anywhere in the a-c plane. Because both a and c show positive expansion and β (obtuse) increases with increasing temperature, the axis of greatest expansion in this plane must lie in the acute β angle (inset, Fig. 3). There appears to be a discontinuity in cell dimensions between 720° and 760°C, particularly along the direction of greatest thermal expansion. Although the thermal expansion data are not conclusive proof of a first-order transition, they do indicate that the transition occurs at a discrete temperature and are consistent with either a first- or second-order transition.

Figures 1 and 2 yield an insight into the nature of the *P*-to-*C* transition. The $h + k$ odd diffractions remain sharp and observable right up to the temperature of the transition, decreasing gradually in intensity with respect to the $h + k$ even diffractions.

TABLE 3. Occupancies, Fractional Coordinates, and Isotropic Temperature Factors for Clinohypersthene at Several Temperatures

		20°C $P2_1/c$	200°C $P2_1/c$	400°C $P2_1/c$	600°C $P2_1/c$	700°C $P2_1/c$	760°C C2/c	825°C C2/c
M1	Mg Occ.	.497(4)	.520(8)	.522(8)	.507(14)	.524(14)	.521(13)	.503(12)
	Fe Occ.	.503(4)	.480(8)	.478(8)	.493(14)	.476(14)	.479(13)	.497(12)
	X	.2506(1)	.2502(4)	.2501(4)	.2499(11)	.2466(23)	0	0
	Y	.6539(1)	.6535(3)	.6529(3)	.6520(6)	.6522(10)	.9006(6)	.9014(6)
	Z	.2263(2)	.2278(6)	.2297(6)	.2333(12)	.2319(23)	1/4	1/4
	B	.34(3)	.75(7)	1.07(8)	1.83(18)	1.53(15)	1.92(18)	1.99(18)
M2	Mg Occ.	.134(4)	.116(8)	.114(8)	.129(14)	.112(14)	.115(13)	.133(12)
	Fe Occ.	.834(4)	.852(8)	.854(8)	.839(14)	.857(14)	.853(13)	.835(12)
	Ca Occ	.032(F)	.032(F)	.032(F)	.032(F)	.032(F)	.032(F)	.032(F)
	X	.2569(1)	.2566(3)	.2553(3)	.2534(10)	.2539(19)	0	0
	Y	.0154(1)	.0151(2)	.0146(2)	.0141(5)	.0142(7)	.2628(5)	.2630(4)
	Z	.2230(1)	.2251(5)	.2263(5)	.2296(10)	.2326(20)	1/4	1/4
	B	.54(2)	1.04(8)	1.46(8)	2.16(16)	2.36(17)	2.80(18)	2.76(18)
SiA	X	.0439(1)	.0440(4)	.0442(4)	.0435(9)	.0431(17)	.2965(4)	.2967(3)
	Y	.3396(2)	.3395(5)	.3391(5)	.3405(15)	.3479(25)	.0888(6)	.0893(5)
	Z	.2894(2)	.2882(7)	.2845(7)	.2833(12)	.2783(21)	.2690(6)	.2698(6)
	B	.25(3)	.71(8)	.89(8)	1.05(10)	1.26(10)	1.67(11)	1.58(10)
SiB	X	.5524(1)	.5519(4)	.5512(5)	.5503(10)	.5514(17)		
	Y	.8355(2)	.8358(5)	.8364(5)	.8359(18)	.8280(25)		
	Z	.2377(2)	.2393(7)	.2432(5)	.2444(13)	.2520(25)		
	B	.23(3)	.69(8)	.96(9)	1.66(12)	1.44(11)		
O1(A)	X	.8679(4)	.8690(11)	.8691(12)	.8681(27)	.8624(45)	.1234(11)	.1240(9)
	Y	.3378(4)	.3391(12)	.3388(12)	.3431(37)	.3326(59)	.0899(14)	.0901(12)
	Z	.1812(5)	.1757(17)	.1748(17)	.1656(30)	.1567(55)	.1544(13)	.1567(12)
	B	.39(8)	1.2(2)	1.1(2)	1.3(3)	1.5(3)	2.0(2)	1.8(2)
O2(A)	X	.1235(4)	.1257(10)	.1248(12)	.1271(32)	.1241(31)	.3788(13)	.3783(12)
	Y	.4976(4)	.4939(11)	.4926(11)	.4918(26)	.4916(36)	.2407(11)	.2403(11)
	Z	.3354(5)	.3416(17)	.3429(18)	.3394(33)	.3429(38)	.3630(16)	.3619(14)
	B	.46(9)	0.9(2)	1.3(2)	1.9(3)	1.6(2)	2.6(2)	2.7(2)
O3(A)	X	.1039(4)	.1035(10)	.1019(11)	.0997(24)	.1035(25)	.3510(14)	.3510(12)
	Y	.2703(4)	.2660(10)	.2636(10)	.2623(17)	.2631(20)	.0092(10)	.0098(9)
	Z	.5929(5)	.5874(17)	.5811(19)	.5801(33)	.5666(36)	.0483(17)	.0493(14)
	B	.49(9)	1.0(2)	1.2(2)	2.0(3)	1.9(3)	3.8(3)	3.3(3)
O1(B)	X	.3762(4)	.3752(11)	.3753(12)	.3783(25)	.3828(32)		
	Y	.8363(4)	.8370(12)	.8378(12)	.8325(32)	.8406(41)		
	Z	.1332(5)	.1345(16)	.1345(17)	.1361(31)	.1457(39)		
	B	.48(8)	1.0(2)	1.0(2)	1.9(3)	2.3(3)		
O2(B)	X	.6313(4)	.6323(12)	.6327(13)	.6290(33)	.6325(35)		
	Y	.9838(4)	.9809(12)	.9827(13)	.9825(28)	.9841(37)		
	Z	.3822(5)	.3829(18)	.3812(19)	.3799(35)	.3795(40)		
	B	.59(9)	1.4(2)	1.8(3)	1.9(3)	2.0(4)		
O3(B)	X	.6054(4)	.6045(10)	.6023(11)	.6020(24)	.6001(24)		
	Y	.7007(4)	.7047(10)	.7081(10)	.7116(22)	.7129(23)		
	Z	.4724(5)	.4758(16)	.4828(17)	.4937(32)	.5048(25)		
	B	.39(8)	0.6(2)	0.8(2)	2.3(5)	2.2(4)		

* Fixed

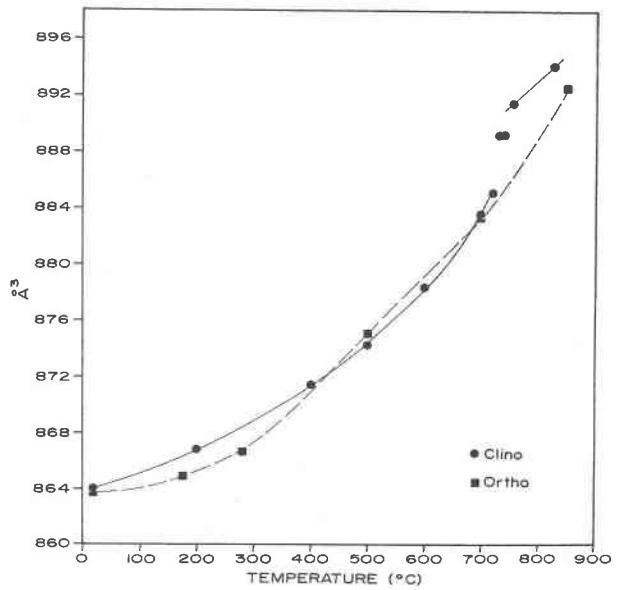

FIG. 3. Cell volumes of ortho and clinohypersthene as a function of temperature. The slopes are nearly parallel and coincident up to 700°C, when the slope of the curve for clinohypersthene becomes steeper and discontinuous at the transition to $C2/c$. Above the transition, the curve for the monoclinic form has the lower slope and the two curves appear to cross somewhere between 850° and 900°C.

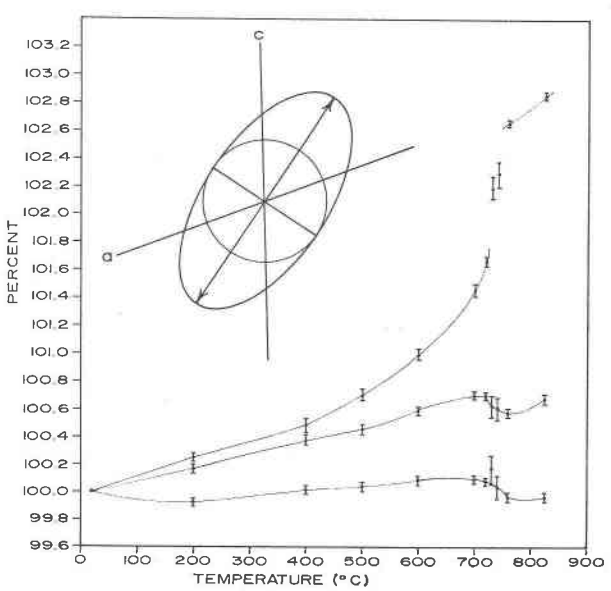

FIG. 4. Plot of the principal axes of the thermal expansion ellipsoids calculated between 20°C and each of the temperatures at which cell dimensions were measured, on the basis of percent expansion. The inset shows the approximate orientation of the major and minor axes in the a-c plane. The length of the major axis, located between 30° and 40° from c in the acute β angle, indicates a discontinuity at the transition from $P2_1/c$ to $C2/c$ at 725°C.

The profile of *102* at 725°C was taken as close as possible to the temperature of the inversion, and appears to be broken. Similar behavior for $30\bar{4}$ and *702* is interpreted as resulting from the crystal having crossed the transition several times as the peak was being scanned. Temperature fluctuations during the scan are estimated to have been less than 2°C. There was no evidence whatever of the $h + k$ odd diffraction at 730°C. The apparently vertical sides of the breaks in the $h + k$ odd scans at the transition indicate that the transition is first-order, and that there is a discontinuous isothermal change taking place in the structure.

The structures on either side of the transition reveal further evidence of a discrete isothermal change occurring at the transition. Figure 5 is a plot of the chain axis angle (O3-O3-O3) for clinopyroxene and orthopyroxene, and shows the straightening of the silicate chains in response to the differential expansion of the polyhedra in both the orthopyroxene and clinopyroxene structures. Figure 5 also demonstrates the topologic difference between the two structures, namely the differing sense of rotation of the A-type

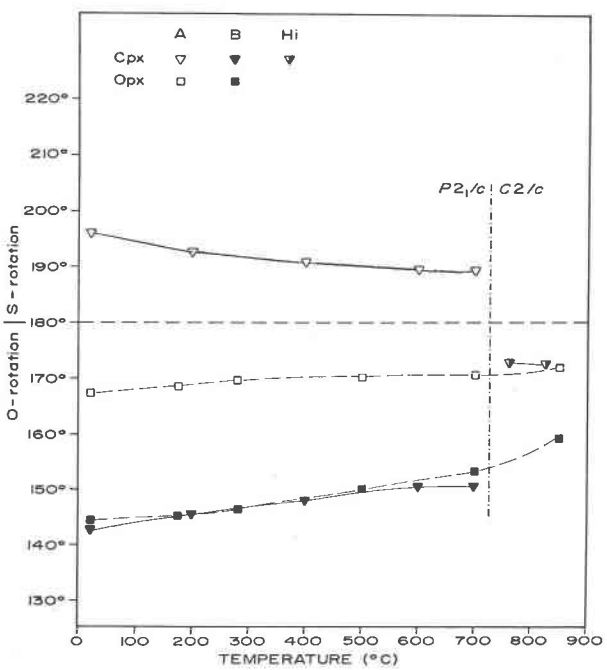

FIG. 5. Chain axis angles for ortho- and clinohypersthene as a function of temperature. S-rotation is denoted by an axis angle greater than 180° as in the A-chain of clinohypersthene. At the transition from $P2_1/c$ to $C2/c$ the A-chain rotates through 180° to become O-rotated in the $C2/c$ structure.

silicate chains.[4] As the temperature is increased, the *S*-rotated *A* chains in the $P2_1/c$ pyroxene gradually straighten, reaching 190° at 700°C, but at 725°C this angle flips through 180° to 172° in the high temperature $C2/c$ structure. This figure shows that the transition occurs at a discrete temperature rather than gradually.

Prewitt *et al* (1971) report that it is difficult to assign a discrete temperature to the high-low transition in lunar calcic pigeonites because of the hysteresis effects in the Fe-rich samples, and because the intensities of the $h + k$ odd diffractions decreased gradually with increasing temperature. It may be that the non-uniform distribution of Ca due to zoning and augite exsolution in the natural specimens are causing the transition to occur over a range of temperatures. In contrast, the Ca-content of the current specimen is considerably lower, and is expected to be of uniform distribution, which may account for the differences observed in the nature of the transition. As was discussed in the introduction, selective diffuseness of subsymmetry diffractions has been generally attributed to the small size of domains over which short-range order of the low symmetry cell is maintained. If a reaction on cooling to a lower symmetry cell is of the first order, then the time allowed for nucleation and growth of the subsymmetry domains will be small at all cooling rates, and it is more likely that other factors such as crystal defects or exsolution lamellae may exert more control on the domain size than the cooling rate will. This hypothesis is consistent with the observation that no selective diffuseness of the $h + k$ odd diffractions was observed at any temperature up to 725°C or after cooling across the transition at different rates. Brown *et al* (1972a) observed increased diffuseness of the $h + k$ odd diffraction after quenching Mull pigeonite (En_{39} Fs_{52} Wo_9) from 960°C (30°C above the transition temperature for this composition), and observed that the *P-C* transition occurred at progressively lower temperatures after prolonged heating. Such a hysteresis effect may be due primarily to homogenization of submicroscopic Ca-rich lamellae with heating. Theoretically one would expect a first-order transition of this nature to result in a two phase field of finite width in temperature-composition space. However, diffusion rates may be too slow to realize the two-phase field experimentally or in nature without encountering the reconstructive inversion to orthopyroxene.

Topology

In observing the effects of temperature on clinohypersthene, it is very useful to compare the structure refinements with those of orthohypersthene, in which no analogous transition takes place, so that the effects of topology and temperature can be separated. At 20°C, the orthopyroxene structure is very similar to that of low clinopyroxene, and the various cations in the two structures have nearly identical first-neighbor coordinations. Looking at the structures of each as a set of layers in the *b-c* plane, the tetrahedra labeled *B* (SiB, O1B, O2B, O3B, nomenclature of Burnham *et al,* 1967) form a layer of silicate chains, and the entire layers are nearly identical in the two structures. Likewise the *M*-cation layers on either side of the *B*-silicate layer will almost perfectly superimpose in a^* projection. The topologic difference between the two structures arises in the layers of tetrahedra labeled *A* (SiA, O1A, O2A, O3A). While an a^* projection of one *A*-chain from the clino structure will nearly superimpose on an ortho *A*-chain, the entire *b-c* layer of chains will not, because the symmetry element relating adjacent chains within a given *A*-layer is different in the two different structures. In the orthorhombic structure, adjacent *A*-chains are related by a *b*-glide plane normal to *a* bisecting the layers of *A*-chains, while in the $P2_1/c$ monoclinic structure, adjacent *A*-chains are related by a 2_1 axis parallel to *b* and lying in the plane of the chains. The 2_1 axis results in the *A* chains of clino having the opposite rotation sense (Thompson, 1970; Papike *et al,* 1973) from those of ortho, so that the low clino *A* chains have an *S*-rotation, and those of ortho an *O*-rotation. The topologic difference allows the monoclinic $P2_1/c$ structure to be capable of a displacive increase in symmetry to $C2/c$; however, the orthorhombic structure is not because *Pbca* is not a subgroup of a higher-symmetry space group. As the temperature is increased, the divalent cation bonds to oxygen expand, while the stronger Si–O bonds do not; but because of the topologic difference between the two structures, this differential expansion affects the structures in quite different ways. This becomes clear as we examine the behavior of each of the cation polyhedra. Cation-

[4] In low clinohypersthene, the *A* chains are nearly straight, but slightly *S*-rotated, while the *B* chains are more strongly kinked with an *O*-rotation. For a definition of *S*- and *O*-rotations, see Thompson (1970) and Papike and Ross (1970; Fig. 1).

oxygen distances and the chain axis angles (O3-O3-O3) at each temperature are presented in Table 4.

Differential Expansion of Cation-Oxygen Bonds

A plot of the percent expansion of the mean cation-oxygen distances in the various coordination polyhedra (Fig. 6) clearly shows the differential in thermal expansion between Si–O bonds and the other cation-oxygen bonds in the structure. This differential, which has been noted in previous high temperature structural studies on pyroxenes (Smyth, 1971; Sueno, Cameron, and Prewitt, 1973; Cameron *et al,* 1973; Smyth and Burnham, 1972; *etc*), is due to the fact that the stretching modes of the stronger Si–O bonds are not excited below about 700°C, whereas the stretch of the weaker *M*–O bonds is excited at much lower temperatures. The oxygens,

TABLE 4. Cation-Oxygen Distances and Chain Axis Angles

	20°C $P2_1/c$	200°C $P2_1/c$	400°C $P2_1/c$	600°C $P2_1/c$	700°C $P2_1/c$	760°C C2/c	825°C C2/c
Tetrahedral							
SiA - 01A	1.616(2)	1.609(4)	1.610(4)	1.618(7)	1.631(8)	1.602(6)	1.603(6)
- 02A	1.597(2)	1.580(4)	1.573(4)	1.571(6)	1.592(8)	1.587(6)	1.587(6)
- $03A_1$	1.658(2)	1.653(4)	1.643(4)	1.642(7)	1.649(8)	1.618(6)	1.636(6)
- $03A^1$	1.629(2)	1.625(4)	1.624(4)	1.638(7)	1.620(8)	1.655(6)	1.670(6)
Average of 4	1.625	1.617(4)	1.613(4)	1.617(7)	1.623(8)		
Average Bridging (2)	1.644	1.639	1.634	1.640	1.635		
Average Non-bridging (2)	1.607	1.595	1.592	1.595	1.611		
SiB - 01B	1.618(2)	1.624(4)	1.618(4)	1.587(6)	1.560(8)		
- 02B	1.601(2)	1.582(4)	1.589(4)	1.581(6)	1.560(8)		
- $03B_1$	1.684(2)	1.667(4)	1.664(4)	1.676(7)	1.699(8)		
- $03B^1$	1.657(2)	1.658(4)	1.648(4)	1.618(7)	1.604(8)		
Average of 4	1.640	1.633	1.630	1.616	1.606		
Average Bridging (2)	1.671	1.663	1.656	1.647	1.652		
Average Non-bridging (2)	1.610	1.603	1.604	1.584	1.560		
Average of 8	1.633	1.625	1.621	1.616	1.614	1.615	1.624
Average Bridging (4)	1.657	1.651	1.645	1.644	1.643	1.637	1.653
Average Non-bridging (4)	1.608	1.599	1.598	1.589	1.586	1.595	1.595
03A-03A-03A Angle	195.9°	192.6°	190.7°	189.6°	189.4°	172.8°	172.4°
03B-03B-03B Angle	142.5°	145.3°	147.8°	150.4°	150.2°		
Octahedral							
M1 - 01A	2.155(3)	2.183(5)	2.188(5)	2.235(8)	2.235(9)	2.257(8)	2.254(8)
- $01A^1$	2.074(2)	2.057(5)	2.065(5)	2.039(8)	2.026(8)	2.081(8)	2.091(7)
- 02A	2.065(2)	2.085(5)	2.098(5)	2.070(8)	2.091(8)	2.090(8)	2.103(8)
- $01B_1$	2.187(3)	2.197(5)	2.216(5)	2.217(9)	2.226(9)		
- $01B^1$	2.088(2)	2.085(5)	2.080(5)	2.085(8)	2.113(9)		
- 02B	2.094(2)	2.117(5)	2.103(5)	2.136(8)	2.110(9)		
Average (6)	2.111	2.121(5)	2.125(5)	2.130(8)	2.134(9)	2.143	2.149
M2 - 01A	2.156(3)	2.162(5)	2.158(5)	2.128(8)	2.108(9)	2.146(8)	2.148(8)
- 02A	2.029(2)	2.002(4)	2.003(5)	2.021(8)	1.987(10)	1.997(8)	2.002(8)
- 03A	2.394(3)	2.434(5)	2.465(5)	2.487(9)	2.504(11)	2.682(9)	2.686(8)
- 01B	2.121(2)	2.115(5)	2.122(5)	2.195(9)	2.225(10)		
- 02B	2.002(2)	1.987(4)	1.994(5)	2.001(8)	1.990(9)		
- $03B_1$	2.543(3)	2.599(5)	2.674(6)	2.766(10)	2.833(12)	3.245(9)	3.249(9)
- $03B^1$	3.079(3)	3.047(5)	3.024(7)	2.987(10)	2.926(12)		
Average of 4	2.077	2.067	2.069	2.086	2.077	2.071	2.075
Average of 6	2.208	2.217	2.236	2.266	2.275	2.368	2.373
Average of 6	2.297	2.291	2.294	2.303	2.290	2.275	2.279

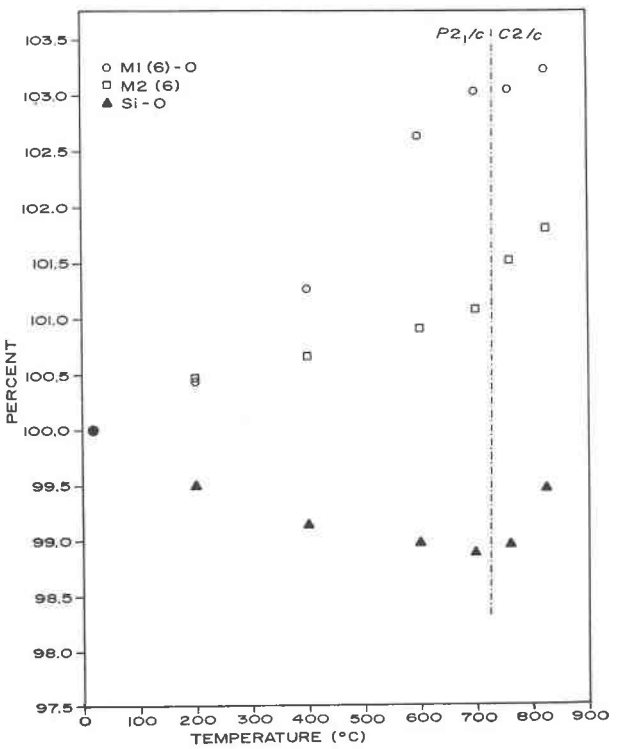

FIG. 6. Percent expansion of the mean cation-oxygen distances for *M*1, *M*2, and Si. This figure illustrates the major difference in thermal expansion between *M* cations and Si.

as their bonding to the *M* cations decreases with increasing temperature, increase their bonding to Si so that the Si–O distances show a slight decrease up to about 700°C, above which the Si–O distances begin to increase with increasing temperature. It is this prominent differential in expansion between the units of the structures which is the driving force for the major structural changes with temperatures, and which brings about the inversion to the high temperature form.

The M1 Octahedron

In light of the zero to slightly negative thermal expansion of the Si–O bonds, it is the thermal expansion of the *M*–O bonds which gives rise to the structural changes with temperatures. The mean *M*1–O bond lengths in orthopyroxene and clinopyroxene at various temperatures are plotted in Figure 7. The differences in *M*1–O bond lengths between the two structures below 500°C most likely reflect the differing Mg and Fe contents of the site. Although the two crystals studied have the same composition, they have different thermal histories, and Fe-Mg distribution equilibrium is not established in orthopyroxene below about 500°C (Virgo and Hafner, 1969, 1970). The orthopyroxene had not previously been heated, while the clinopyroxene had been quenched from 900°C, so that below 500°C the clinopyroxene had more of the larger Fe^{2+} cations in *M*1 than the orthopyroxene. Above 500°C, the equilibrium Fe-Mg distribution should have been attained before intensity measurement commenced, at least in orthopyroxene (Virgo and Hafner, 1969). The most important feature of Figure 8 is, however, the apparent jump in the mean *M*1–O distances as the monoclinic structure goes from $P2_1/c$ to $C2/c$. Even though Table 3 indicates a slightly smaller Fe content of *M*1 in clinopyroxene than Smyth (1973) found in orthopyroxene of the same composition at a corresponding temperature, the *M*1 site of high clinopyroxene appears to be slightly larger than that of orthopyroxene.

The M2 Polyhedron

The mean *M*2–O distances in ortho- and clinopyroxene, plotted at several temperatures (Fig. 8), clearly show the effects of the $P2_1/c$ to $C2/c$ transition. In both $P2_1/c$ and $C2/c$, the *M*2 cation is coordinated by six oxygens; however at the transition, one O3B atom leaves the coordination polyhedron, and another enters. The differences in mean *M*2–O

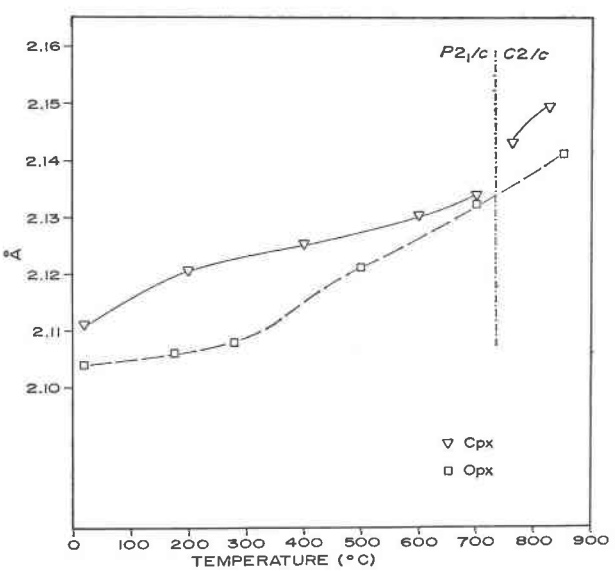

FIG. 7. Mean *M*1–O distances for ortho- and clinohypersthene at several temperatures.

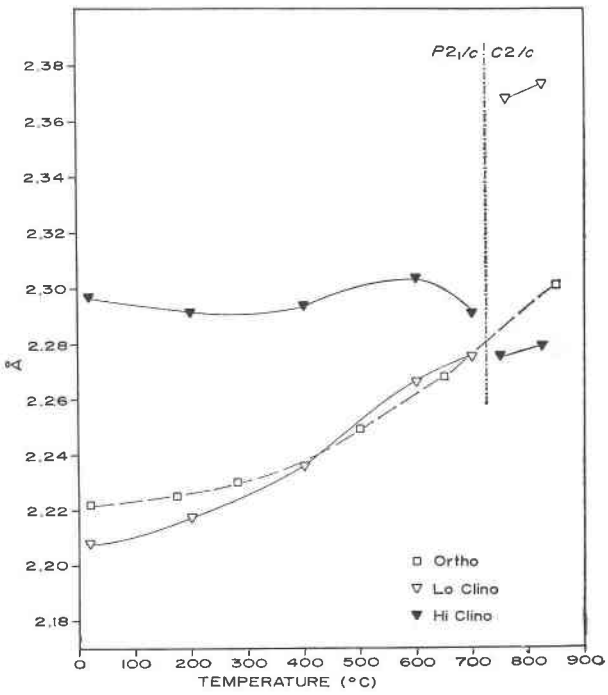

FIG. 8. Mean $M2$–O distances for ortho- and clinohypersthene at several temperatures. The solid triangles indicate the mean distance to the six oxygens which coordinate $M2$ in the $C2/c$ structure while the open triangles indicate the mean distance to the six oxygens which coordinate $M2$ in the $P2_1/c$ structure. The vertical dotted line indicates the transition temperature (725°C).

distances between low clino- and orthopyroxene reflect the fact that the $M2$ site in clino contained more Mg and less Fe than in orthopyroxene below 500°C. At 725°C, there is an apparent discontinuous change in the coordination of $M2$ as one $M2$–O3 bond is broken and another formed. It is important to note that the $M2$ site of high clinopyroxene is slightly smaller than that of orthopyroxene at corresponding temperatures, and that this difference is not in the sense which one would expect from the relative Mg contents of the two sites.

Cation Ordering

The degree of Mg-Fe ordering has been used to estimate cooling rates of many lunar and terrestrial pigeonites (Finger *et al,* 1972; Hafner and Virgo, 1970; Hafner, Virgo, and Warburton, 1971; Schürmann and Hafner, 1972; Ghose, Ng, and Walter, 1972; Ghose and Wan, 1973; Gay, Bancroft, and Bown, 1970; Schürmann, Anderson, and Hafner, 1971; Brown and Wechsler, 1973; Dowty, Ross, and Cuttitta, 1972). These studies have been based upon the ΔG_E determined by Mössbauer spectroscopy of heated natural pigeonites (Hafner, Virgo, and Warburton, 1971; Schürmann and Hafner, 1972), and to a lesser extent, on an X-ray determination by Brown *et al* (1972a). These experiments are summarized in Table 5. These authors obtained values of ΔG_E for Fe-Mg exchange between $M1$ and $M2$ in pigeonites from 4.1 to 4.9 kcal/mole in the range 500° to 1000°C. This is a slightly larger value than was obtained for orthopyroxene in the same temperature range, indicating that the clinopyroxenes tend to be more ordered. Dowty *et al* (1972) raise the possibility of a bias in the Mössbauer data on clinopyroxenes, particularly high-Ca clinopyroxenes, which would tend to give anomalously large amounts of Fe in $M2$, thereby indicating a higher degree of order. Further, Mössbauer determinations are so few that it is impossible to estimate the effects on ΔG_E of Ca content, total Fe/Fe + Mg ratio for the crystal, or the P to C transition.

Results of the current study of cation-ordering are presented in Table 5 along with similar results for pigeonites of Schürmann and Hafner (1972) and Brown *et al* (1972a), and for orthopyroxene of Smyth (1973), Schürmann and Hafner (1972), and Virgo and Hafner (1969). The results for the current study agree very well with those for 12021 pigeonite, but less well with those for 14053 pigeonite and Mull pigeonite. All clinopyroxenes observed in-

TABLE 5. Distribution Coefficients and Mg-Fe Exchange Energies of Low Ca Pyroxenes

Pyroxene	Composition En	Fs	Wo	T(°C)	k*	ΔG_E Kcal/mole	Reference
Clinopyroxenes							
12021,150	59	32	9	555	0.08		**
				800	0.15	4.1	**
				1000	0.18	4.3	**
14053,47	58	30	12	1000	0.16	4.7	***
Mull	39	52	9	960	0.14	4.9	†
B1-9	31	67	1.5	700	0.11	4.2	this work
				760	0.12	4.3	this work
				825	0.16	4.0	this work
Orthopyroxenes							
B1-9	31	67	1.5	500	0.08	4.0	††
				700	0.14	3.8	††
				850	0.18	3.8	††
14310,116	70	24	6	1000	0.21	4.0	***
3209-40	42	56	2	600	0.12	3.7	†††
3209-45				700	0.14	3.8	†††
3209-36				800	0.18	3.6	†††
3209-27				1000	0.22	3.9	†††

* $k = (Fe/Mg)_{M1}/(Fe/Mg)_{M2}$
** Hafner et al. (1971)
*** Schürmann and Hafner (1972)
† Brown et al. (1972)
†† Smyth (1973)
††† Virgo and Hafner (1969)

dicate slightly more ordering (*i.e.*, larger ΔG_E) than do orthopyroxenes at corresponding temperatures, in agreement with the conclusions of Brown *et al* (1972a) and Schürmann and Hafner (1972). However, the current study further shows that the difference is not entirely due to the additional Ca in clinopyroxene creating a larger energy differential between the two sites. This is clear because the ortho and clino that have the same composition also show a slight difference in ΔG_E. The close agreement between the current study ($Wo_{1.5}$) and the 12021 pigeonite (Wo_9) may indicate that Ca has little effect on ΔG_E; however, the large ΔG_E observed by Brown *et al* (1972a) for Mull pigeonite (Wo_9) may indicate that Ca has a considerable effect. The results of the current study also confirm the conclusion of Schürmann and Hafner (1972) that no great variation in ΔG_E occurs across the $P2_1/c$ to $C2/c$ inversion. However, we may be seeing the beginning of a decrease in ΔG_E with increasing temperature at 825°C. Certainly this may be expected because in the $C2/c$ form, the $M1$ and $M2$ sites are more similar in size than they are in the orthorhombic form at an equivalent temperature (Figs. 7, and 8). Further study of ordering in pigeonites at elevated temperatures is needed to substantiate such a trend.

Thermal Parameters

Figure 9 is a plot of the equivalent isotropic temperature factors (B) for $M1$ and $M2$ and the mean B for Si and for the oxygens. The magnitudes and orientations of the principal axes of the thermal vibration ellipsoids are presented in Table 6. Because the anisotropic temperature factors of the oxygens in the $P2_1/c$ structure at 700°C were not positive-definite (did not define an ellipse), and the equivalent isotropic temperature factors showed somewhat erratic behavior near the transition, an attempt was made to refine the 700°C structure in space group $C2/c$. This attempt yielded a large R of 0.18 and very large isotropic temperature factors for Si and O. Likewise, an attempt was also made to refine the 760°C structure in space group $P2_1/c$, which resulted in coordinates of the atoms of the A and B chains which were not significantly different from their positions in the $C2/c$ structure. These experimental refinements further strengthen the conclusions of Brown *et al* (1972a) and Ohashi (1973) that the $C2/c$ structure is real and does not represent the dynamic average of the two chain configurations of a $P2_1/c$ structure. Further, they indicate that the $P2_1/c$ structure is also real, and that a first-order

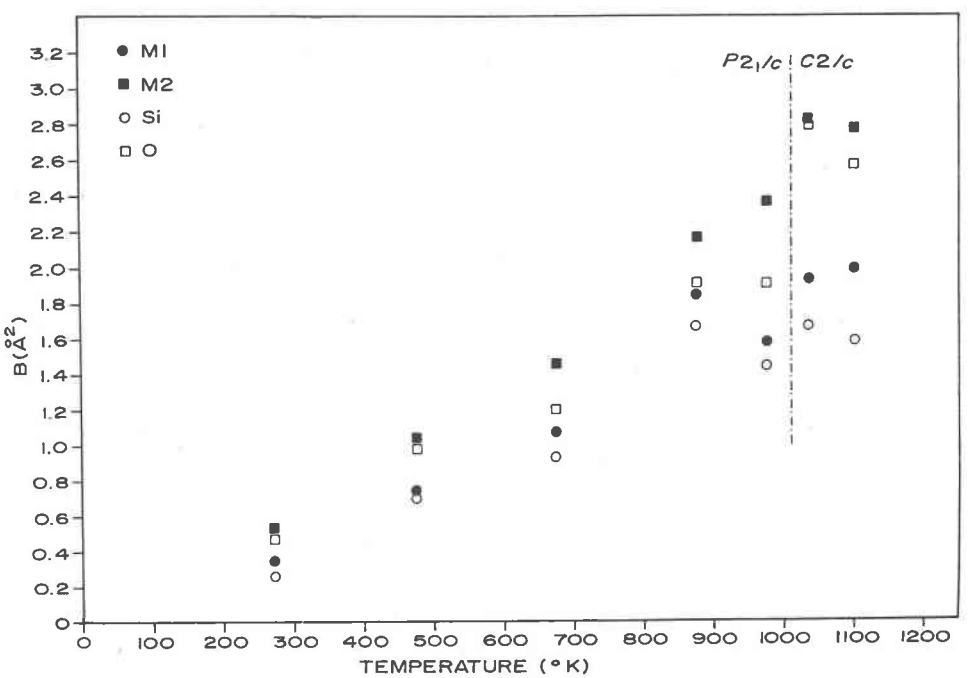

FIG. 9. The isotropic temperature factor, B, in Å² for $M1$ and $M2$ and the mean B for Si and O as a function of temperature in clinohypersthene.

transition takes place between the two at about 725°C.

Conclusions

The most important conclusion of this study is that the transition from $P2_1/c$ to $C2/c$ in clinopyroxenes is of the first order. This conclusion is based upon three independent lines of evidence. First, the $h + k$ odd diffractions remain sharp and observable right up to the inversion temperature and abruptly disappear at 725°C. Second, the cell dimensions appear to undergo a discontinuous change at the inversion temperature. Third, structure refinements 30°C on either side of the transformation result in structures which are drastically different. Further, the high temperature structure in space group $C2/c$ appears to be a real structure, that is, the single silicate chain does not appear to be a time or space average of the two chains of a disordered primitive structure.

Because the transition is first order, it appears that the relative diffuseness of the $h + k$ odd diffractions observed in some higher Ca pigeonites is likely to be more a function of Ca content than cooling rate. Structure refinements of high clinopyroxene indicate that the $M1$ site is slightly larger, and $M2$ slightly smaller, than in orthopyroxene at the same temperature. Despite the slightly greater similarity in the two sites of high clino, there is a slight tendency for the high clinopyroxenes to exhibit more ordering of Mg and Fe on $M1$ and $M2$, and for Fe-Mg exchange to begin at higher temperatures and have a higher ΔG of exchange than in orthopyroxene. Comparison of the cation ordering measurements with those of previous studies indicates that the $P2_1/c$ to $C2/c$ transi-

TABLE 6. Amplitudes and Orientations of Principal Axes of Thermal Vibration Ellipsoids

Temp.	Axis	RMS Ampl. r_i (Å)	Angle of r_i with axis a	b	c	RMS Ampl. r_i (Å)	Angle of r_i with axis a	b	c	RMS Ampl. r_i (Å)	Angle of r_i with axis a	b	c
Atom			M1				M2				Si(A)		
20°C	1	0.044(1)	164(7)	82(6)	58(7)	0.072(1)	54(4)	108(4)	59(4)	0.039(2)	7(4)	94(5)	102(5)
	2	0.053(1)	92(6)	37(7)	123(7)	0.084(1)	64(5)	131(5)	136(5)	0.062(2)	90(4)	149(20)	119(19)
	3	0.066(1)	74(7)	54(7)	50(6)	0.092(1)	133(5)	133(5)	63(5)	0.065(2)	97(5)	121(21)	32(20)
200°C	1	0.061(2)	138(7)	96(7)	31(8)	0.098(2)	110(7)	92(8)	2(7)	0.082(4)	28(20)	63(18)	111(20)
	2	0.099(2)	130(7)	69(8)	116(7)	0.115(2)	140(9)	54(7)	90(8)	0.087(4)	88(21)	103(19)	159(20)
	3	0.122(2)	81(8)	22(8)	75(8)	0.130(2)	57(8)	36(8)	88(7)	0.112(4)	62(15)	149(17)	87(18)
400°C	1	0.086(2)	53(7)	142(7)	92(8)	0.123(2)	82(14)	89(14)	27(12)	0.087(4)	140(16)	93(15)	32(16)
	2	0.108(2)	57(8)	75(8)	159(7)	0.129(2)	115(12)	25(14)	80(13)	0.106(4)	129(17)	81(16)	121(18)
	3	0.147(2)	54(8)	55(7)	69(7)	0.155(2)	153(8)	115(7)	65(8)	0.123(4)	86(16)	10(17)	83(16)
600°C	1	0.095(6)	51(14)	39(14)	99(15)	0.140(5)	67(9)	34(13)	76(12)	0.063(6)	56(18)	34(17)	100(18)
	2	0.147(6)	96(14)	82(15)	153(15)	0.152(5)	89(10)	65(15)	150(12)	0.123(6)	117(19)	71(15)	129(17)
	3	0.198(6)	140(15)	52(16)	65(15)	0.198(5)	157(8)	69(8)	64(9)	0.144(6)	134(18)	63(17)	41(16)
700°C	1	0.098(5)	123(14)	144(15)	68(15)	0.099(5)	69(10)	130(9)	58(10)	**			
	2	0.140(6)	112(14)	90(14)	139(15)	0.186(5)	42(14)	104(13)	146(15)				
	3	0.174(6)	139(16)	54(15)	58(15)	0.217(5)	56(13)	43(14)	80(14)				
760°C	1	0.136(5)	77(12)	90(*)	33(12)	0.159(5)	82(15)	90(*)	28(14)	0.135(5)	60(25)	30(28)	104(28)
	2	0.159(5)	90(*)	180(*)	90(*)	0.187(5)	90(*)	180(*)	90(*)	0.138(5)	58(24)	112(25)	154(23)
	3	0.171(5)	167(13)	90(*)	57(12)	0.214(5)	172(15)	90(*)	62(13)	0.162(5)	47(15)	110(14)	68(14)
850°C	1	0.131(5)	95(12)	90(*)	15(11)	0.154(5)	86(12)	90(*)	24(12)	0.126(5)	115(22)	81(23)	10(22)
	2	0.165(5)	90(*)	180(*)	90(*)	0.181(5)	90(*)	180(*)	90(*)	0.135(5)	118(22)	152(24)	85(21)
	3	0.177(5)	5(12)	90(*)	105(12)	0.219(5)	176(11)	90(*)	66(11)	0.161(5)	39(14)	117(15)	82(15)
Atom											Si(B)		
20°C	1									0.039(2)	24(4)	81(6)	86(5)
	2									0.055(2)	75(6)	60(6)	108(5)
	3									0.067(2)	109(5)	108(6)	18(7)
200°C	1									0.063(4)	41(16)	49(16)	104(17)
	2									0.087(4)	73(17)	110(18)	160(18)
	3									0.122(4)	54(12)	133(13)	76(13)
400°C	1									0.090(4)	128(20)	123(22)	42(24)
	2									0.097(4)	93(21)	134(28)	132(24)
	3									0.138(4)	38(14)	118(13)	83(15)
600°C	1									0.071(6)	126(18)	64(18)	33(20)
	2									0.142(6)	135(19)	83(17)	115(18)
	3									0.195(6)	112(18)	153(19)	70(17)
700°C	1									0.106(6)	144(27)	91(24)	35(23)
	2									0.116(6)	112(25)	139(21)	113(27)
	3									0.253(6)	63(18)	130(17)	65(16)

* *Fixed by symmetry constraints of space group C2/c.*
** *Temperature factor of this atom is not positive-definite.*

TABLE 6, Continued

Temp.	Axis	RMS Ampl. r_i (Å)	Angle of r_i with axis a	b	c	RMS Ampl. r_i (Å)	Angle of r_i with axis a	b	c	RMS Ampl. r_i (Å)	Angle of r_i with axis a	b	c
		O1(A)				O2(A)				O3(A)			
20°C	1	0.038(5)	22(14)	75(16)	92(14)	0.029(7)	143(15)	126(14)	72(14)	0.049(7)	141(15)	113(17)	45(18)
	2	0.076(6)	87(18)	51(25)	139(29)	0.088(6)	61(16)	135(21)	130(19)	0.079(7)	123(18)	88(20)	128(21)
	3	0.089(6)	112(17)	43(27)	49(28)	0.096(6)	70(18)	113(20)	45(22)	0.101(7)	108(18)	23(19)	71(20)
200°C	1	0.096(10)	87(20)	120(22)	37(21)	0.074(11)	165(20)	89(22)	56(24)	0.078(13)	22(21)	73(23)	95(24)
	2	0.123(12)	160(28)	109(28)	79(23)	0.112(12)	97(30)	157(31)	108(26)	0.107(14)	69(21)	123(24)	146(22)
	3	0.140(11)	110(30)	37(33)	55(21)	0.122(12)	77(29)	113(29)	40(25)	0.144(12)	84(21)	142(20)	57(22)
400°C	1	0.080(11)	80(21)	130(21)	50(23)	0.059(12)	107(22)	29(20)	62(21)	0.094(12)	122(31)	41(30)	58(25)
	2	0.114(12)	63(24)	128(23)	139(21)	0.142(13)	24(28)	68(23)	117(29)	0.116(14)	148(32)	120(29)	84(24)
	3	0.153(12)	30(23)	63(25)	96(24)	0.156(12)	73(30)	108(23)	40(27)	0.152(14)	86(24)	115(23)	33(22)
600°C	1	0.040(18)	125(31)	133(+)	52(+)	0.053(17)	110(29)	34(32)	58(33)	0.102(18)	23(32)	75(34)	92(36)
	2	0.143(18)	89(32)	124(+)	142(+)	0.139(18)	153(30)	99(34)	96(30)	0.135(18)	68(30)	112(35)	157(34)
	3	0.170(17)	35(31)	118(30)	87(29)	0.227(18)	106(31)	123(30)	33(29)	0.220(20)	83(29)	153(30)	67(32)
700°C	1	**				**				0.085(19)	134(34)	128(35)	54(33)
	2									0.122(22)	56(36)	142(38)	115(33)
	3									0.203(22)	62(29)	88(30)	47(32)
760°C	1	0.136(15)	91(36)	92(32)	20(38)	0.115(16)	81(29)	16(30)	80(28)	0.146(18)	159(29)	79(33)	53(29)
	2	0.156(17)	131(34)	139(34)	79(37)	0.171(17)	35(28)	89(32)	145(29)	0.171(19)	109(30)	97(32)	140(29)
	3	0.181(19)	139(32)	50(30)	74(34)	0.236(18)	56(28)	106(31)	57(31)	0.306(23)	98(29)	167(31)	77(30)
825°C	1	0.140(15)	89(32)	8(28)	83(31)	0.134(15)	104(28)	43(29)	47(28)	0.113(16)	113(29)	78(30)	27(28)
	2	0.154(16)	71(+)	83(31)	173(+)	0.177(15)	47(29)	53(27)	129(29)	0.169(17)	137(30)	102(31)	111(29)
	3	0.158(16)	19(+)	93(33)	91(+)	0.228(17)	47(27)	110(26)	69(28)	0.279(19)	89(28)	163(30)	74(29)
		O1(B)				O2(B)				O3(B)			
20°C	1	0.064(6)	66(23)	25(22)	104(17)	0.068(6)	114(16)	66(17)	25(18)	0.044(7)	137(18)	115(17)	42(16)
	2	0.070(6)	141(22)	74(20)	106(19)	0.085(7)	69(16)	27(15)	112(17)	0.072(7)	119(19)	104(19)	130(19)
	3	0.097(6)	118(18)	71(19)	22(17)	0.103(6)	33(17)	101(17)	78(18)	0.089(6)	161(22)	150(20)	100(18)
200°C	1	0.072(11)	97(21)	82(25)	14(21)	0.063(11)	143(24)	110(25)	43(28)	0.049(12)	72(24)	72(27)	41(25)
	2	0.112(12)	137(24)	133(23)	76(24)	0.135(11)	100(25)	131(26)	129(27)	0.080(12)	35(23)	67(28)	131(24)
	3	0.137(11)	48(26)	136(27)	93(25)	0.171(12)	55(23)	132(24)	75(25)	0.117(13)	61(25)	150(27)	92(26)
400°C	1	0.070(13)	46(28)	44(30)	98(34)	0.095(12)	115(27)	117(28)	29(27)	0.074(13)	125(31)	66(32)	31(30)
	2	0.090(12)	80(32)	93(31)	170(33)	0.141(13)	147(28)	97(30)	103(29)	0.107(14)	84(29)	26(30)	115(29)
	3	0.161(12)	45(28)	134(27)	95(28)	0.197(13)	110(28)	28(26)	65(27)	0.187(15)	36(24)	81(25)	74(26)
600°C	1	0.110(18)	28(31)	116(31)	98(37)	0.080(19)	121(30)	145(29)	67(34)	0.069(19)	145(34)	70(36)	46(34)
	2	0.154(19)	106(32)	140(33)	118(35)	0.144(18)	50(34)	123(34)	136(33)	0.171(21)	108(38)	66(35)	136(33)
	3	0.188(17)	112(32)	118(34)	29(33)	0.215(20)	55(34)	98(37)	55(35)	0.234(23)	61(37)	32(32)	86(37)
700°C	1	**				**				0.068(19)	150(34)	62(37)	63(38)
	2									0.132(20)	114(35)	115(38)	130(41)
	3									0.244(26)	108(37)	141(37)	52(40)

+ Orientation of this axis is essentially indeterminate as expected when cross section of thermal ellipsoid is nearly circular.

tion has only a minor effect upon ΔG_E, while the effect of Ca content on ΔG_E may be significant.

Acknowledgments

The author thanks Dr. Russell B. Merrill of the Lunar Science Institute, Drs. Robin Brett and Richard J. Williams of NASA-Johnson Space Center, and Professor Charles W. Burnham of Harvard University for helpful reviews. Three data collections (20°C, 200°C, and 400°C) were performed at Harvard University and supported by NSF Grant GA-12852 to Professor Burnham. The remainder of the study was supported by the Lunar Science Institute which is operated by the Universities Space Research Association under contract No. NSR 09-051-001 with the National Aeronautics and Space Administration. This paper constitutes the Lunar Science Institute Contribution No. 180.

References

BROWN, G. E., C. T. PREWITT, J. J. PAPIKE, AND S. SUENO (1972a) A comparison of the structures of low and high pigeonite. *J. Geophys. Res.* **77,** 5778–5789.

———, J. J. PAPIKE, AND C. T. PREWITT (1972b) The relationship of domain structure in pigeonites to thermal history and the $P2_1/c \rightleftarrows C2/c$ transition (abstr.). *Geol. Soc. Am. Abstr. Programs* **4,** 458–459.

———, AND B. A. WECHSLER (1973) Crystallography of pigeonites from basaltic vitrophyre 15597. *Proc. Fourth Lunar Sci. Conf., Geochim. Cosmochim. Acta Suppl. 4,* **1,** 887–900.

BURNHAM, C. W. (1966) Computation of absorption correction and the significance of end effect. *Am. Mineral.* **51,** 159–167.

———, J. R. CLARK, J. J. PAPIKE, AND C. T. PREWITT (1967) A proposed crystallographic nomenclature for clinopyroxene structures. *Z. Kristallogr.* **125,** 109–119.

———, Y. OHASHI, S. S. HAFNER, AND D. VIRGO (1971) Cation distribution and atomic thermal vibrations in an iron-rich orthopyroxene. *Am. Mineral.* **56,** 850–876.

CAMERON, M., S. SUENO, C. T. PREWITT, AND J. J. PAPIKE (1973) High temperature crystal chemistry of acmite, diopside, hedenbergite, jadeite, spodumene, and ureyite. *Am. Mineral.* **58,** 594–618.

CROMER, D. T., AND J. B. MANN (1968) X-ray scattering factors computed from numerical Hartree-Fock wave functions. *Acta Crystallogr.* **24,** 321–324.

DOWTY, E., M. ROSS, AND F. CUTTITTA (1972) Fe^{2+}-Mg site distribution in Apollo 12021 pyroxenes: Evidence for bias in Mössbauer measurements and relation of ordering to exsolution. *Proc. Third Lunar Sci. Conf., Geochim. Cosmochim. Acta Suppl. 3,* **1,** 481–492.

FINGER, L. W. (1969) Determination of cation distribution by least squares refinement of single crystal X-ray data. *Carnegie Inst. Wash. Year Book,* **67,** 216–217.

———, S. S. HAFNER, K. SCHÜRMANN, D. VIRGO, AND D. WARBURTON (1972) Distinct cooling histories and reheating of Apollo 14 rocks. *Lunar Science III,* Ed., C. Watkins, *Lunar Sci. Inst. Contrib.* No. **88,** 259–261.

FOIT, F. F., AND D. R. PEACOR (1973) The anorthite crystal structure at 410° and 830°C. *Am. Mineral.* **58,** 665–675.

GAY, P., G. M. BANCROFT, AND M. G. BOWN (1970) Diffraction and Mössbauer studies of minerals from lunar soils and rocks. *Proc. Apollo 11 Lunar Sci. Conf. Geochim. Cosmochim. Acta, Suppl. 1,* **1,** 481–497.

GHOSE, S., G. NG, AND L. S. WALTER (1972) Clinopyroxenes from Apollo 12 and 14, exsolution, domain structure, and cation order. *Proc. Third Lunar Sci. Conf., Geochim. Cosmochim. Acta Suppl. 3,* **1,** 481–492.

———, AND C. WAN (1973) Luna 20 pyroxenes: Evidence for a complex thermal history. *Proc. Fourth Lunar Sci. Conf. Geochim. Cosmochim. Acta Suppl. 4,* **1,** 901–907.

HAFNER, S. S., AND D. VIRGO (1970) Temperature dependent cation distributions in lunar and terrestrial pyroxenes. *Proc. Apollo 11 Lunar Sci. Conf. Geochim. Cosmochim. Acta Suppl. 1,* **3,** 2183–2198.

———, ———, AND D. WARBURTON (1971) Cation distributions and cooling history of clinopyroxenes from Oceanus Procellarum. *Proc. Second Lunar Sci. Conf., Geochim. Cosmochim. Acta, Suppl. 2,* **1,** 91–108.

MORIMOTO, N. (1956) The existence of monoclinic pyroxenes with the space group C^5_{2h} — $P2_1/c$. *Proc. Jap. Acad.* **32,** 750–752.

———, D. E. APPLEMAN, AND H. T. EVANS (1960) The crystal structures of clinoenstatite and pigeonite. *Z. Kristallogr.* **114,** 120–147.

———, AND M. TOKONAMI (1969) Domain structure of pigeonite and clinoenstatite. *Am. Mineral.* **54,** 725–740.

OHASHI, Y. (1973) *High Temperature Structural Crystallography of Synthetic Pyroxenes (Ca,Fe)SiO_3.* Ph.D. Thesis, Harvard University.

———, AND C. W. BURNHAM (1973) Clinopyroxene lattice deformations: The roles of chemical substitution and temperature. *Am. Mineral.* **58,** 843–849.

PAPIKE, J. J., AND M. ROSS (1970) Gedrites: crystal structures and intracrystalline cation distributions. *Am. Mineral.* **55,** 1945–1972.

———, C. T. PREWITT, S. SUENO, AND M. CAMERON (1973) Pyroxenes: comparisons of real and ideal structural topologies. *Z. Kristallogr.* **69,** 254–273.

PREWITT, C. T., J. J. PAPIKE, AND M. ROSS (1970) Cummingtonite: a reversible, nonquenchable transition from $P2_1/m$ to $C2/m$ symmetry. *Earth Planet. Sci. Lett.* **8,** 448–450.

———, G. E. BROWN, AND J. J. PAPIKE (1971) Apollo 12 clinopyroxenes: High temperature X-ray diffraction studies. *Proc. Second Lunar Sci. Conf. Geochim. Cosmochim. Acta, Suppl. 2,* **1,** 59–68.

SCHÜRMANN, K., AND S. S. HAFNER (1972) Distinct subsolidus cooling histories of Apollo 14 basalts. *Geochim. Cosmochim. Acta, Suppl. 3,* **1,** 493–506.

———, A. T. ANDERSON, AND S. S. HAFNER (1972) Mg,Fe order-disorder in ortho- and clinopyroxenes from a Hawaiian lava flow (abstr.). *Trans. Am. Geophys. Union,* **53,** 541.

SMITH, J. V. (1969) Magnesium pyroxene at high temperature: inversion in clinoenstatite. *Nature,* **222,** 256–257.

SMYTH, J. R. (1969) Orthopyroxene-high-low-clinopyroxene inversions. *Earth Planet. Sci. Lett.* **6,** 406–407.

——— (1971) Protoenstatite: a crystal structure refinement at 1100°C. *Z. Kristallogr.* **134,** 262–272.

——— (1972) A simple heating stage for single-crystal diffraction studies up to 1000°C. *Am. Mineral.* **57,** 1305–1309.

——— (1973) An orthopyroxene structure up to 850°C. *Am. Mineral.* **58,** 636–648.

——— (1974) Experimental study on the polymorphism of enstatite. *Am. Mineral.* **59,** 345–352.

———, AND C. W. BURNHAM (1972) The crystal structures of high and low clinohypersthene. *Earth Planet. Sci. Lett.* **14,** 183–189.

SUENO, S., M. CAMERON, AND C. T. PREWITT (1973) The orthoferrosilite structure (abstr.). *Geol. Soc. Am. Abstr. Programs,* **5,** 829–830.

THOMPSON, J. B. (1970) Geometrical possibilities for amphibole structures: model biopyriboles. *Am. Mineral.* **55,** 292–293.

VIRGO, D., AND S. S. HAFNER (1969) Fe^{2+},Mg order-disorder in heated orthopyroxenes. *Mineral. Soc. Am. Spec. Pap.* **2,** 67–81.

———, AND ——— (1970) Fe^{2+},Mg order-disorder in natural orthopyroxenes. *Am. Mineral.* **55,** 201–223.

Manuscript received, February 20, 1974; accepted for publication, May 13, 1974.